Resolution enhancement in digital holographic microscopy with structured illumination

Jun Ma (马 骏)[1], Caojin Yuan (袁操今)[2*], Guohai Situ (司徒国海)[3], Giancarlo Pedrini[4], and Wolfgang Osten[4]

[1]*School of Electronic and Optical Engineering, Nanjing University of Science and Technology, Nanjing 210094, China*

[2]*Department of Physics, Nanjing Normal University, Nanjing 210097, China*

[3]*Shanghai Institute of Optics and Fine Mechanics, Chinese Academy of Sciences, Shanghai 201800, China*

[4]*Institut für Technische Optik, Universität Stuttgart, Pfaffenwaldring 9, 70569 Stuttgart, Germany*

[*]*Corresponding author: caojin.yuan@gmail.com*

Received May 4, 2013; accepted June 28, 2013; posted online September 3, 2013

We present a digital holographic microscope wherein the sample is illuminated by structured light to enable the capture of additional object spatial frequencies. Reconstructed images with increased spatial resolution are obtained by separating and synthesizing bandwidths of different frequency regions in the Fourier domain. The theoretical analysis and experimental results are presented.

OCIS codes: 090.0090, 090.1995, 110.0110, 110.0180.

doi: 10.3788/COL201311.090901.

Digital holographic microscopy (DHM)[1−4] is a powerful imaging tool for studying microstructures, biological cells, and particles. The lateral resolution of DHM is given by $k\lambda/\mathrm{NA_{eff}}$, where $\mathrm{NA_{eff}}=\mathrm{NA_{ill}}+\mathrm{NA_{obj}}$ is the effective numerical aperture (NA) of the recording system, which is the sum of the NAs of the illumination and the objective[5−7]; λ is the wavelength of the light source; k is a proportional constant determined by the system configuration.

Several digital holographic systems based on the synthetic aperture have been proposed to improve microscope resolutions. Holograms containing different ranges of spatial frequencies are obtained by shifting the camera or rotating the sample. After synthesizing frequencies into a large-aperture hologram[8,9], high-resolution reconstructions can be achieved. However, this method is time-consuming and requires high set-up stability. Mico *et al.*[10,11] proposed several systems to improve resolution using vertical-cavity surface-emitting laser (VCSEL) light sources and spatial multiplexing techniques instead of moving the camera or the object. However, holograms covering different frequency regions are still recorded sequentially. Two or more holograms can be angularly multiplexed into one frame[12,13], but the recording set-ups of such systems are complex because many beam splitters or mirrors are required to produce several references and object illumination beam pairs with different carrier frequencies. Inserting a grating into the path of the object in the holographic system shifts higher-frequency information into the recording range, which simplifies the set-up[14,15]. Many gratings with different periods, however, must be prepared according to the target. Paturzo *et al.*[16] utilized an electro-optical two-dimensional (2D) tunable grating to improve the resolution of the reconstructed images, but this method required a reduction in the object field of view due to the large pixel size of the electro-optical grating. Structured illumination is widely used to improve the resolution in microscopy, and at least three images are required to separate the overlapped information in each direction by shifting the phase of the grating[17−20].

In this letter, we present an approach to improve the resolution of a digital holographic microscope using frequency-adjustable structured light. The proposed system allows the recording of not only object information as on-axis illumination but also additional frequencies in two directions in one step and without any physical variation of the system. The proposed system is thus easy to implement. In comparison with a system using traditional structured illumination, the additional frequency in the proposed system can be separated from low-frequency information by subtraction so that fewer recordings are required. The complex amplitude of the reconstructed image is obtained by synthesizing high and low frequencies. Moreover, the spatial frequency information of the recorded object is adjustable and allows tuning of the resolution.

The proposed digital holographic system is a modified Mach-Zehnder interferometer, as shown in Fig. 1. A plane wave obtained by expanding and collimating a laser beam is divided into reference and object beams by the beam splitter $\mathrm{BS_1}$. The illuminated object (O) is magnified by a microscope objective (MO) and brought to the recording plane. The reference wave, reflected by $\mathrm{M_2}$ and $\mathrm{BS_2}$, interferes with the object wavefront, and a charge coupled device (CCD) detector is used to record the interference pattern. In the reference arm, a lens $\mathrm{L_3}$ is inserted to compensate for the wavefront curvature

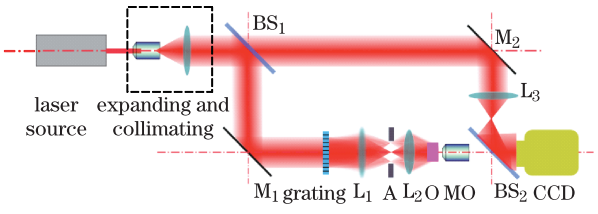

Fig. 1. Experimental setup. M: mirror; BS: beam splitter; A: aperture.

introduced by the MO.

When the sample is illuminated by an on-axis plane wave (NA_{ill}=0), the resolution of the system is $k\lambda/NA_{eff}$=$k\lambda/NA_{obj}$. As in conventional microscopy, the resolution of a digital holographic microscope may be improved by increasing the NA of the illumination (NA_{ill}), which can be done by the introduction of a scattering plate. The illumination has a random unknown phase, and determination of the phase change after reconstruction of the digital hologram will not be possible because of the sample. Furthermore, the reconstructed intensity is speckled. To avoid these effects, we illuminate the sample using structured light with a well-defined amplitude and phase distribution; this light is obtained by imaging a grating onto the sample using a system composed of lenses L_1 and L_2 (Fig. 1). Between L_1 and L_2, an aperture (A) exists; this aperture is used to select the spatial frequency of the structured light and obtain on-axis illumination when the aperture diameter is small.

We consider an object illuminated by structured coherent light with a well-defined amplitude and phase distribution. We perform a complete analysis of the illumination of the object with a 2D periodical fringe pattern produced by imaging a grating and described by

$$t(x_O, y_O) = 1 + \frac{m}{2}\cos\left(2\pi\frac{x_O}{p_x}\right) + \frac{m}{2}\cos\left(2\pi\frac{y_O}{p_y}\right), \quad (1)$$

where p_x and p_y are the periods of the grating along the x and y directions, respectively, and m is the coefficient of the first diffraction order. If we denote the transmission of the object by $O(x_O, y_O)$, we obtain

$$\begin{aligned} O'(x_O, y_O) &= O(x_O, y_O)t(x_O, y_O) \\ &= O(x_O, y_O)\Big\{1 + \frac{m}{4}\Big[\exp\Big(-\mathrm{i}2\pi\frac{x_O}{p_x}\Big) \\ &\quad + \exp\Big(\mathrm{i}2\pi\frac{x_O}{p_x}\Big) + \exp\Big(-\mathrm{i}2\pi\frac{y_O}{p_y}\Big) \\ &\quad + \exp\Big(\mathrm{i}2\pi\frac{y_O}{p_y}\Big)\Big]\Big\} \\ &= O'_0 + O'_{x-} + O'_{x+} + O'_{y-} + O'_{y+}. \end{aligned} \quad (2)$$

After passing through the MO, the five diffraction orders (O_{x-}, O_{x+}, O_{y-}, O_{y+}, and O_0) interfere with the reference beam R. The intensity of the interference (hologram) is given by

$$\begin{aligned} I_1(x,y) &= (O_{x-} + O_{x+} + O_0 + O_{y-} + O_{y+} + R)(O_{x-} \\ &\quad + O_{x+} + O_0 + O_{y-} + O_{y+} + R)^* \\ &= |O_{x-}|^2 + |O_{x+}|^2 + |O_0|^2 + |O_{y-}|^2 + |O_{y+}|^2 \\ &\quad + |R|^2 + O_{x-}(O_{x+} + O_0 + O_{y-} + O_{y+})^* \\ &\quad + O_{x+}(O_{x-} + O_0 + O_{y-} + O_{y+})^* + O_0(O_{x-} \\ &\quad + O_{x+} + O_{y-} + O_{y+})^* \\ &\quad + O_{y-}(O_{x-} + O_{x+} + O_0 + O_{y+})^* + O_{y+}(O_{x-} \\ &\quad + O_{x+} + O_0 + O_{y-})^* \\ &\quad + R^*(O_{x-} + O_{x+} + O_0 + O_{y-} + O_{y+}) \\ &\quad + R(O_{x-} + O_{x+} + O_0 + O_{y-} + O_{y+})^*, \end{aligned} \quad (3)$$

and its Fourier transform (FT) is

$$\widetilde{I}_1(f_x, f_y) = \widetilde{A}(f_x, f_y) + \widetilde{C}(f_x, f_y) + \widetilde{U}(f_x, f_y) + \widetilde{U}^*(f_x, f_y), \quad (4)$$

where $\widetilde{A}(f_x, f_y) = \mathrm{FT}[|O_{x-}|^2 + |O_{x+}|^2 + |O_0|^2 + |O_{y-}|^2 + |O_{y+}|^2 + |R|^2]$ and $\widetilde{C}(f_x, f_y)$ is the FT of the cross-correlation between O_0 and O_{x-}, O_{x+}, O_{y-}, O_{y+}. The third term in Eq. (4) is

$$\begin{aligned} \widetilde{U}(f_x, f_y) &= \widetilde{O}(f_x - \Delta F_x, f_y - \Delta F_y) \\ &\quad + \Big[\widetilde{O}\Big(f_x - \Delta F_x - \frac{M}{p_x}, f_y - \Delta F_y\Big) \\ &\quad + \widetilde{O}\Big(f_x - \Delta F_x + \frac{M}{p_x}, f_y - \Delta F_y\Big) \\ &\quad + \widetilde{O}\Big(f_x - \Delta F_x, f_y - \Delta F_y - \frac{M}{p_y}\Big) \\ &\quad + \widetilde{O}\Big(f_x - \Delta F_x, f_y - \Delta F_y + \frac{M}{p_y}\Big)\Big], \end{aligned} \quad (5)$$

where the factor M has been inserted to take the magnification of the imaging system into account and ΔF_x and ΔF_y are the carrier frequencies of the reference beam. $\widetilde{U}^*(f_x, f_y)$ is the complex conjugate of $\widetilde{U}(f_x, f_y)$.

The spectrum $\widetilde{I}(f_x, f_y)$ is shown in Fig. 2(a). $\widetilde{A}(f_x, f_y)$ and $\widetilde{C}(f_x, f_y)$ are located around the center of the Fourier domain, and $\widetilde{U}(f_x, f_y)$ and $\widetilde{U}^*(f_x, f_y)$ are displaced to (ΔF_x, ΔF_y) and (-ΔF_x, -ΔF_y), respectively; these parameters can be separated by applying spectral filtering. Figure 2(b) shows that $\widetilde{U}(f_x, f_y)$ is the sum of the object spectrum and its four replicas produced by 2D periodic pattern illuminations. The offset distances of the replica components are given by the frequencies M/p_x and M/p_y. A one-dimensional (1D) sketch of

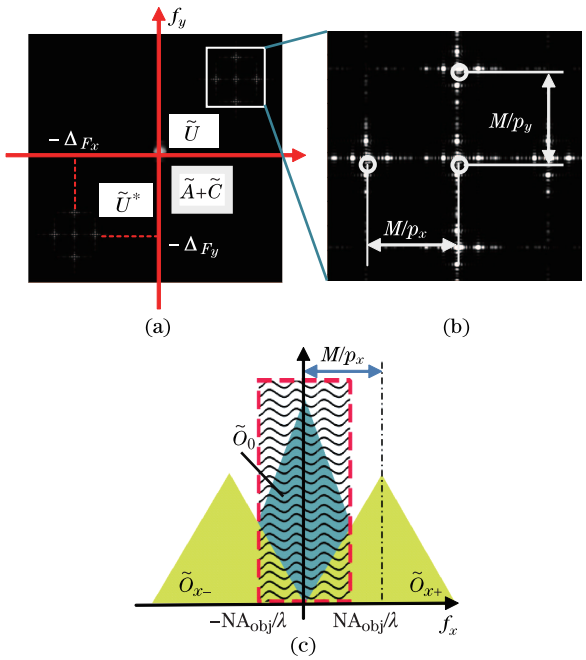

Fig. 2. Schematic representations of (a) $\widetilde{I}(f_x, f_y)$ and (b) $\widetilde{U}(f_x, f_y)$; (c) the 1D frequency bandwidth of $\widetilde{U}(f_x, f_y)$.

$\widetilde{U}(f_x, f_y)$ is given in Fig. 2(c), which shows that the system only allows passage of the frequency components within the range [–$\mathrm{NA_{obj}}/\lambda$, $\mathrm{NA_{obj}}/\lambda$]. Therefore, the system accepts not only the low-frequency component of $\widetilde{O}_0$ but also the high-frequency components of $\widetilde{O}_{x+}$ and $\widetilde{O}_{x-}$ because of structured illumination. $\widetilde{O}_{x+}$ and $\widetilde{O}_{x-}$ usually overlap with $\widetilde{O}_0$. However, if we assume that no overlap occurs between $\widetilde{O}_{x-}$, $\widetilde{O}_{x+}$, $\widetilde{O}_{y-}$, and $\widetilde{O}_{y+}$, these components can be separated from $\widetilde{O}_0$ by performing the subtraction $\widetilde{I}_1(f_x, f_y) - \widetilde{I}_2(f_x, f_y)$, where $\widetilde{I}_2(f_x, f_y) = \mathrm{FT}\{|O_0|^2 + |R|^2 + O_0R^* + O_0^*R\}$ is the spectrum of the hologram $I_2(x, y)$ recorded by on-axis illumination.

To obtain the correct reconstruction of the object wavefront, shifting the four high-frequency components by M/p_x or M/p_y and setting them back to their original positions in the spatial frequency domain is necessary (see 1D sketch in Fig. 3(a)). Shifting of these components to the center of the frequency domain to compensate ΔF is also necessary. For instance, the carrier frequency of the last term $\widetilde{O}(f_x' - \Delta F_x, f_y' - \Delta F_y + M/p_y)$ in Eq. (5) can be removed by shifting it toward $(\Delta F_x, \Delta F_y - M/p_y)$ in the Fourier domain. This "frequency resetting" must be applied to avoid the appearance of interference patterns in the reconstructed image[13]. The spectrum obtained after resetting and stitching of the low- and high-frequency components is shown in Fig. 3(b). The figure shows that unrecordable object spatial frequencies under on-axis illumination become recordable under structured illumination. In the example shown in Fig. 3, the obtained effective NA (and thus, the system resolution) shows a twofold increase compared with that obtained under on-axis illumination $\mathrm{NA_{eff}}$=2$\mathrm{NA_{obj}}$. The highest spatial frequency recorded is found along the grating orientations[19]. To obtain resolution enhancement in all directions, $|M|^2$ the grating must rotate (e.g., by 45°) and record more holograms.

An experiment using the set-up shown in Fig. 1 was performed. The light source used was a He-Ne laser (λ=633 nm) and digital holograms were recorded by a CCD with 2 452×2 054 pixels (size: 3.45×3.45 (μm)). A lens system formed by L_1 and L_2 (focal lengths: f_1=120 mm, f_2=20 mm) projected a six-time demagnified image of a grating on the object. The spatial frequencies of the grating are 25.2 and 21.0 lp/mm along the x and y directions, respectively, and the frequencies of the demagnified image are 151.2 and 126.0 lp/mm, respectively. The focal length of L_3 is 120 mm and a 3.2× MO with $\mathrm{NA_{obj}}$=0.12 is used to obtain images of the object.

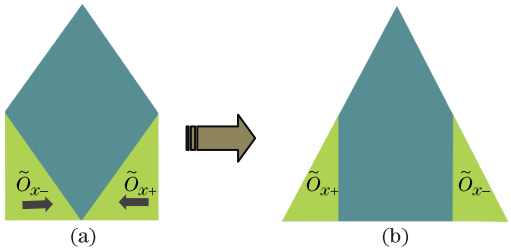

Fig. 3. (a) Shift of the high-frequency components (b) to obtain an enlarged spectrum.

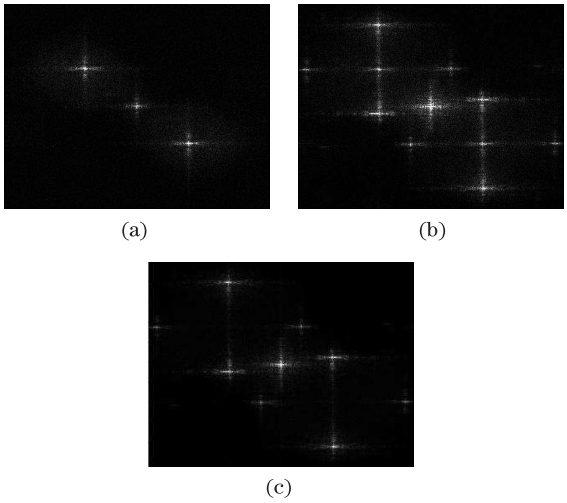

Fig. 4. Spectrum of the hologram under (a) on-axis illumination, (b) structured illumination, and (c) without low frequencies.

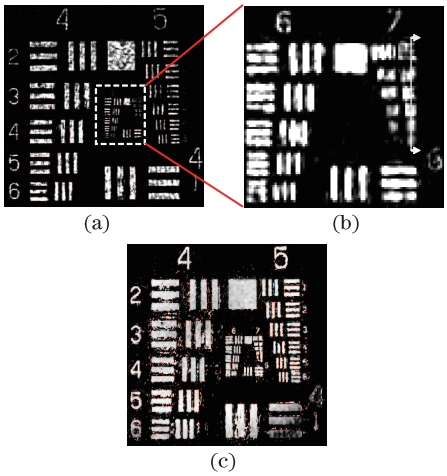

Fig. 5. (a) Intensity distribution under on-axis illumination and (b) magnified area marked within a white square of (a); (c) phase distribution.

Given these parameters, the resolution of the system is $k\lambda/\mathrm{NA_{eff}}$=4.1 μm (k = 0.77[21], $\mathrm{NA_{ill}}$=0 if on-axis coherent illumination is used), which corresponds to the sixth element in Group No. 6 of the USAF1951 test target.

The spectra of the holograms recorded under on-axis and structured illumination are shown in Figs. 4(a) and (b), respectively. From Fig. 4(b), we can see that the object frequencies recorded in a single contain the object spectrum and its four frequency-shifted replicas. Furthermore, low frequencies overlap with high frequencies. To delineate these frequencies, we subtract the low frequencies shown in Fig. 4(a) from the crosstalk frequencies shown in Fig. 4(b) to obtain a spectrum with the four high-frequency components (Fig. 4(c)).

Figure 5 shows the results of the reconstruction of the USAF test target obtained under on-axis illumination. The intensity of the reconstructed image, an enlarged region of this image, and the phase are shown in Figs. 5(a), (b), and (c), respectively. The resolution is 4.38 μm, which corresponds to the sixth element in Group No. 6.

Figure 6 shows regions where the resolution has been improved by superposing the complex amplitude containing low frequencies with the four other complex amplitudes containing high frequencies. Frequency resetting can be done without difficulty because the grating parameters and the four components covering the high-frequency band are known. The resolutions in both vertical and horizontal directions improve from 114.0 lp/mm under on-axis illumination to 228.0 lp/mm under structured illumination.

We also compared the reconstruction results obtained by inserting a random phase plate into the illumination beam, which increases the NA_{ill} and leads to the recording of higher frequencies under structured illumination compared with that obtained under on-axis illumination. Figure 7 shows that the third elements in the seventh group (161.3 lp/mm) can be resolved, but the intensity distributions are non-uniform because of speckles. The phase in Fig. 7(c) is random.

In Fig. 8, intensity plots along the solid lines shown in Figs. 5(b), 6(b), and 7(b) are reported for comparison.

In conclusion, a method for improving the spatial resolution of digital holographic microscopes using structured illumination is proposed. Low- and high-frequency information can be recorded in one step and separated in the Fourier domain. After filtering and application of a reconstruction algorithm, high-resolution images are obtained by synthesizing the complex amplitudes. Compared with previous methods, the proposed system is easy to implement and the resolution is tunable by adjusting the period of the grating rendered visually on the object. The proposed system requires low CCD bandwidth and the phase information of the object can be obtained. The resolution of the reconstructed object with aperture synthesis is improved by a factor of 2 in comparison with the resolution obtained from a system without structured illumination. The resolution could exceed 228.0 lp/mm when structured illuminations of higher frequency are used. The proposed system could be used to investigate small structures, three-dimensional reconstructions with high micro-object resolution, and biological samples.

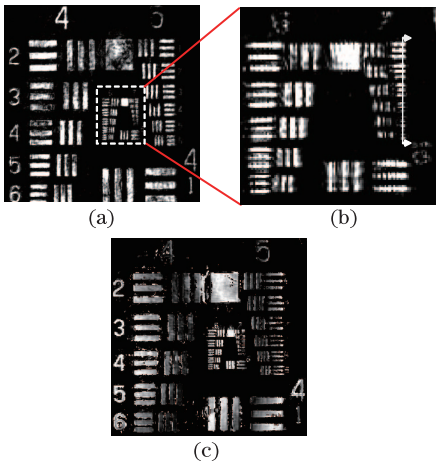

Fig. 6. (a) Intensity distribution under structured illumination and (b) magnified area marked within a white square of (a); (c) phase distribution.

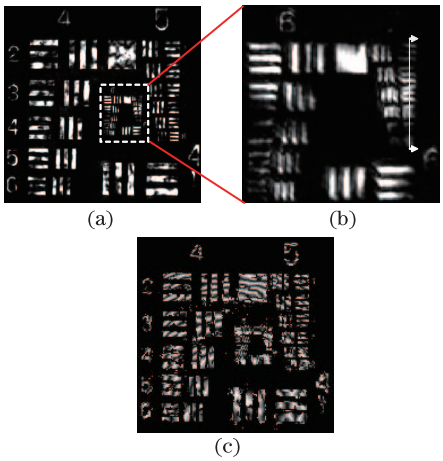

Fig. 7. (a) Intensity distribution under diffuser illumination and (b) magnified area marked within a white square of (a); (c) phase distribution.

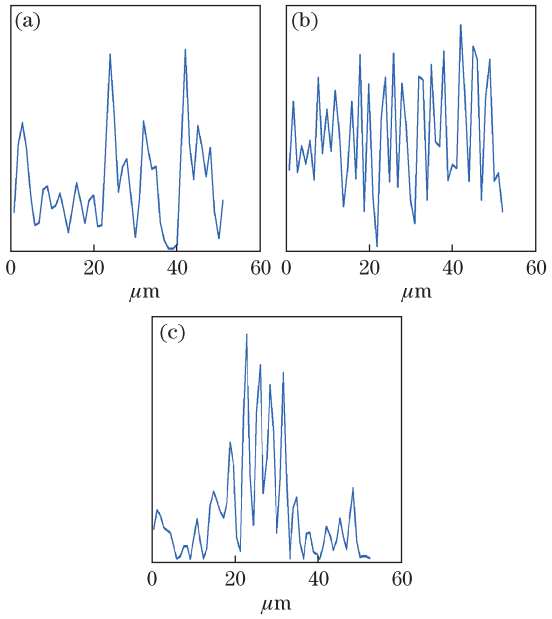

Fig. 8. Plots along the white solid lines shown in Figs. 5(b), 6(b), and 7(b).

This work was supported by the National Natural Science Foundation of China (No. 61205162), the Opening Project of Key Laboratory of Astronomical Optics and Technology, Chinese Academy of Sciences (No. CAS-KLAOT-KF201204), and the Fundamental Research Founds for the Central Universities (No. 30920130111007). C. Yuan gratefully acknowledges the support of the Alexander von Humboldt Foundation.

References

1. X. Wu, G. Gréhan, S. Meunier-Guttin-Cluzel, L. Chen, and K. Cen, Opt. Lett. **34,** 857 (2009).
2. B. Rappaz, F. Charrière, C. Depeursinge, P. J. Magistretti, and P. Marquet, Opt. Lett. **33,** 744 (2008).
3. L. Xu, X. Peng, J. Miao, and A. K. Asundi, Appl. Opt. **40,** 5046 (2001).
4. Y. Wang, D. Wang, J. Zhao, Y. Yang, X. Xiao, and H. Cui, Chin. Opt. Lett. **9,** 030901 (2011).
5. Y. Kuznetsova, A. Neumann, and S. R. J. Brueck, J. Opt. Soc. Am. A **25,** 811 (2008).

6. A. Stern and B. Javidi, Opt. Eng. **43,** 239 (2004).
7. D. P. Kelly, B. M. Hennelly, N. Pandey, T. J. Naughton, and W. T. Rhodes, Opt. Eng. **48,** 095801 (2009).
8. F. Le Clerc, M. Gross, and L. Collot, Opt. Lett. **26,** 1550 (2001).
9. R. Binet, J. Colineau, and J. C. Lehureau, Appl. Opt. **41,** 4775 (2002).
10. V. Mico, Z. Zalevsky, P. García-Martínez, and J. García, Appl. Opt. **45,** 822 (2006).
11. V. Mico, Z. Zalevsky, P. García-Martínez, and J. García, J. Opt. Soc. Am. A **23,** 3162 (2006).
12. C. Yuan, H. Zhai, and H. Liu, Opt. Lett. **33,** 2356 (2008).
13. J. Zhao, X. Yan, W. Sun, and J. Di, Opt. Lett. **35,** 3519 (2010).
14. V. Mico, Z. Zalevsky, and J. García, Opt. Express **14,** 5168 (2006).
15. C. Liu, Z. Liu, F. Bo, Y. Wang, and J. Zhu, Appl. Phys. Lett. **81,** 3143 (2002).
16. M. Paturzo, F. Merola, S. Grilli, S. De Nicola, A. Finizio, and P. Ferraro, Opt. Express **16,** 17107 (2008).
17. S. A. Shroff, J. R. Fienup, and D. R. Williams, J. Opt. Soc. Am. A **26,** 413 (2009).
18. P. Kner, B. B Chhun, E. R Griffis, L. Winoto, and M. G. L. Gustafsson, Nature Methods **6,** 339 (2009).
19. C. Yuan, G. Situ, G. Pedrini, J. Ma, and W. Osten, Appl. Opt. **50,** B6 (2011).
20. L. Chen, Y. He, F. Liu, J. Su, and Y. Yin, Proc. SPIE **5638,** 424 (2005).
21. M. Born and E. Wolf, *Principles of Optics* (Cambridge university press, London, 1999).